Regular Article

Roland T. Loto*

Correlative evaluation of the corrosion resilience and passivation properties of zinc and aluminum alloys in neutral chloride and acid-chloride solutions

https://doi.org/10.1515/eng-2022-0539
received July 30, 2023; accepted October 01, 2023

Abstract: Comparative analysis of the corrosion resilience and passivation characteristics of pure zinc (Zn) and aluminum (Al) alloys in neutral chloride and acid-chloride solutions at 0.5–3% NaCl concentrations was done with potentiodynamic polarization, potentiostatic evaluation, optical characterization, and open circuit potential measurement. Results show Al alloy was more resistant to general corrosion in both solutions with values ranging from 0.031 to 0.082 mm/year, and 0.037 to 0.389 mm/year compared to Zn alloys with values of 0.432–0.691 mm/year and 0.465–5.016 mm/year. Corrosion potential values of Zn alloy were significantly more electronegative than the values for Al alloy. The passivated region of the polarization plots for Al was thermodynamically unstable with visible current transients compared to that of Zn. Passivation of Al occurred at the early onset of anodic polarization in the neutral chloride solution. Zn alloy passivated at specific potentials, coupled with stable passivation behavior. The passivation range values of Al were generally greater than the values for Zn due to delayed stable pitting activity. Optical images for Al showed extensive localized degradation along specific regions and grain boundaries, whereas Zn morphology indicates general surface degradation. Open circuit potential plots indicate significant growth of Al_2O_3 oxide on Al coupled with active–passive transition behavior of the oxide. This contrasts the observation for Zn where the plot configuration indicates limited oxide formation and growth but significant thermodynamic stability.

Keywords: corrosion, passivation, aluminum, zinc, pitting

*** Corresponding author: Roland T. Loto,** Department of Mechanical Engineering, Covenant University, Ota, Ogun State, Nigeria,
e-mail: tolu.loto@gmail.com

1 Introduction

Fe-based alloys have extensive industrial applications worldwide due to their versatility, relative ease of production, availability, and exceptional mechanical properties for applications that require structural rigidity, stiffness, and extended lifespan [1–6]. One of the major limitations in the application of Fe-based alloys is their vulnerability to corrosion, though this is more associated with the carbon-based ferrous alloys whose failure in corrosive environments results in economic and financial loss. Stainless steels with sufficient Cr, Ni, Ti, Mb, etc., content are significantly more resistant to corrosion, but their advantages are offset by their relatively high cost of production and utilization [7–9]. This necessitates the need for low-cost alternatives with respect to corrosion protection of metallic parts, structures, columns, fittings, pipes and components, and mechanical properties. However, other important factors that must be taken into consideration are the cost of production, lower cost of application, etc. [10–13]. The application of Zn coatings has been proven to be one of the most resilient and proven methods of protection of ferrous alloys. This is possible by cold-dip galvanizing, hot-dip galvanizing, galvannealing, electro-galvanizing, continuous-line galvanizing, zinc plating and spraying, mechanical plating, and zinc-pigment paints [14]. Being the fourth most applicable metal worldwide and twenty-third most represented element within the earth's crust (0.013%), about 50% of Zn produced is used in the Zn galvanizing technique [15–17]. The other significant industrial utilization of Zn includes white discoloration in paints, stimulant in rubber processing, manufacture of precautionary agents for rubber polymers and plastics, production of photocopying parts [18,19], catalyst in prototype rockets [20], protective coating for cover sheets, and oil and gas infrastructure [21,22]. Al alloy is extensively utilized in the production of industrial components, civil engineering applications, telecommunication wires, boilers, degradation-resistant containers, chemical

production, and welding of aluminum parts [23]. Al metal makes up about 8% of the elemental composition of the Earth's crust. Its economic importance is second to Fe. The strength and density to mass proportion, electrical and heat conduction, low- and high-temperature stability, non-toxicity, mechanical properties, corrosion resistance, and industrial relevance [24,25]. The aluminum industry yields $174 billion to the American Gross Domestic Product and about $70 billion yearly in direct economic output [26]. Al alloys are significantly applied in the manufacture of parts for vehicles, chemical production plants, energy-generating plants, aeroplanes, infrastructures, etc. [27–30]. The properties of Al can be modified to align distinct industrial and engineering requirements.

The corrosion resistance of Zn is due to the growth of a passive inert oxide film which hinders further corrosion reaction mechanisms when exposed to the atmosphere. The passive inert oxide film occurs due to the reaction of Zn with O_2 resulting in the evolution of $Zn(OH)_2$ and thereafter $ZnCO_3$ after reacting with CO_2 [31]. The electrochemical property of Zn to sustain a protective oxide is mainly determined by the pH of the environment, especially acidic pollutants. Because zinc forms an amphoteric oxide, strong alkalinity can also adversely affect zinc's corrosion behavior by interfering with the formation of protective layers [32]. Salt composition within marine conditions also significantly influences Zn corrosion [33]. Al displays significant resistance to corrosion degradation because of the formation of Al_2O_3 on its surface [34]. Howbeit, its structural strength and functional lifespan can be severely reduced in corrosive environments containing minimal concentrations of Cl, SO_4^{2-}, etc. The protective oxide deteriorates in the presence of threshold concentrations of the corrosive anions [35,36]. A number of theories are available on the mechanism of deterioration of the inert oxide on metallic alloys resulting from the electrolytic transport of reactive species through the protective oxide to the metal. Previous studies show that reactive species interact with the protective oxide leading to its deterioration through the evolution of metallic complexes [37,38]. Other studies suggest deterioration in Cl^- anion electrolyte is related to the intermetallic phase and elemental composition which limits their economic relevance [39]. It has been proven that the protective oxide on metallic alloys is normally stable at minimal anionic concentrations [40–42]. A study on the effect of corrosive anions on Al-based galvanic anodes indicates pitting potential decreased with an increase in anionic content whereas other anionic species showed a passivating effect [43]. Effective utilization of Zn and Al alloys results from adequate information on the corrosive nature of the applicable environments, degradation rate, and type of corrosion. Localized corrosion of Zn and Al can be ascertained by their characteristics, size, microstructural properties, and electrochemical properties at the metal-solution interface This necessitates appropriate comprehension of the nature and process of interaction of the corrosive anions with the metal exterior in aqueous solutions. A number of corrosion resistance studies have been performed on Zn and Al.

Graedel studied the corrosion of Zn in the atmosphere. Observation shows that the corrosion layer formation and the chemical reactions involved are a direct consequence of the pH of the aqueous surface film due to its influence on the dissolution of the passive oxyhydroxide surface [44]. Ferry and Mohd Sukarnoor studied the corrosion reaction processes of Zn-coated mild steel in saline aqueous media. Results showed the degradation rate of fully coated steel reduces with exposure time while the values for the Zn coated with scratch were slightly higher [45]. The atmospheric behavior of hot-dip Zn galvanized and Al-coated steel wire strands from long-term exposure tests in rural sulfur, industrial, and marine areas of the islands of Taiwan was studied by Yaw-Tzong et al. The major corrosion product for the Zn-coated steel in severe marine environments was found to be Fe_2O_3, and no zinc coating was left for the protection of the base steel after 2 years [46]. Al-Moubaraki and Al-Rushud studied the corrosion behavior of Al 7075, Al 2024, and Al 6061 in the Red Sea water. Results obtained showed that the corrosion rates exhibit a continuous decrease with exposure time. The order of corrosivity of the Al alloys is Al 6061 < Al 2024 < Al 7075. Pitting corrosion was the prevalent corrosion pattern detected on alloys [47]. According to Seyeuxa et al. [48], degree of localized corrosion damage differs with regard to the concentration of corrosive species and the type of aqueous environment. There is a need to further evaluate the inert film on metallic alloys to comprehend the mechanism associated with the collapse and reformation of the protective oxides which is the focus of this investigation. Silva et al. [49] and Mollapour and Poursaeidi [50] studied the deterioration of the passive film on stainless steel and established that the strength of the inert oxide to electrochemical degradation is substantially controlled by external factors. In agreement with Pao et al. [51], Zhang et al. [52], Liu et al. [53], and Calderon et al. [54] showed that resistance to pit formation and growth with steel results from different determinant variables associated with industrial environments and metallurgical properties of the alloy. On account of citation [49–54], this research studies the localized corrosion resistance, passivation properties, and polarization behavior of Zn and Al alloys in neutral chloride and acid-chloride solutions.

2 Materials and methods

2.1 Materials and preparation

Flat squared zinc (Zn) sheets with surface proportions of 100 mm by 100 mm by 50 mm (length, breadth, and thickness) and cylindrical aluminum alloy (Al) were cut into six work samples with a median configuration of 1 cm by 1 cm (length and breadth) using manual hand tool for potentiodynamic polarization, optical microscopy, and open circuit potential evaluation. Elemental analysis of the Al and Zn work samples were analyzed with PhenomWorld high-resolution electron microscope. The wt% compositions of Al and Zn are shown in Table 1. Cu cables were affixed to Al and Zn work samples with soft solder before being enmeshed with pre-solidified acrylic paste. The exterior area of the Al and Zn work samples was graded with SiC sheets (60–1,500 grits), brightened with a 3 µm diamond mixture, and washed with de-mineralized H_2O and dimethyl ketone. Neutral chloride solution prepared from recrystallized NaCl (obtained from Titan Biotech, India) at 0.5, 1, 1.5, 2, 2.5, and 3% NaCl concentration. Acid-chloride solution (0.0015 M H_2SO_4 containing 0.5, 1, 1.5, 2, 2.5, and 3% NaCl concentration) was prepared from standard class H_2SO_4 acid solution obtained from Sigma-Aldrich, USA.

2.2 Potentiodynamic polarization and open circuit potential evaluation

Corrosion kinetics was evaluated with potentiodynamic polarization while corrosion thermodynamics was determined by open circuit potential evaluation. Both tests were done at 308 K (ambient temperature) by adopting a Digi-Ivy 2311 potentiostatic apparatus. The apparatus which consists of a triple cord electrode (Al and Zn work sample electrode, Ag/AgCl threshold electrode, and Pt cord counter electrode) was networked to a laptop computer. Polarization data lines were produced at plot progression of 0.0015 V/s initiating at −2 to +0.75 V. Corrosion potential, C_p (V), and corrosion current density C_j (A/cm^2) results were acquired by Tafel computation. Corrosion rate C_r (mm/year) was retrieved from the numerical values below;

$$C_{RT} = \frac{0.00327 \times C_j \times C_q}{D}. \quad (1)$$

Here, E_w indicates the equivalent weight (g) of Al and Zn, 0.00327 represents corrosion constant while D is the density (g/cm^3). Polarization resistance P_{rt}, (Ω) was assessed from the following numerical formula:

$$P_{rt} = 2.303\frac{B_a B_c}{B_a + B_c}\left(\frac{1}{I_{cr}}\right), \quad (2)$$

where B_a and B_c indicate anodic and cathodic Tafel curves (V/dec).

2.3 Optical microscopy analysis

Optical illustrations of Al and Zn work samples prior to and following potentiostatic analysis in neutral chloride and acid-chloride media at specific NaCl concentrations were obtained and studied with an Omax trinocular metallurgical microscope.

3 Results and discussion

3.1 Potentiodynamic polarization studies

The potentiodynamic polarization plots for Al and Zn alloy corrosion in neutral chloride and chloride sulfate electrolytes are shown in the following figures. Figure 1(a) and (b) demonstrates the corrosion polarization plots for Al and Zn alloys in neutral chloride media (0.5–3% NaCl concentration) while Figure 2(a) and (b) illustrates the corrosion polarization plots for Al and Zn alloys in 0.0015 M H_2SO_4 media at 0.5–3% NaCl concentration in 0.0015 M H_2SO_4 solution. Tables 2 and 3 presents the polarization data obtained for both alloys from the neutral chloride and

Table 1: Wt.% Composition of Al and Zn alloys

Element	Fe	Si	Cu	Zn	Ti	Mg	Pb	Sn	Al
Al alloy									
Wt% composition	0.232	0.078	0.0006	0.0016	0.006	0.0027	0.0012	0.007	99.66
Element	**Fe**	**Si**	**Cu**	**Zn**	**Ti**	**Mg**	**Pb**	**Sn**	**Al**
Zn alloy									
Wt% composition	—	—	—	100	—	—	—	—	—

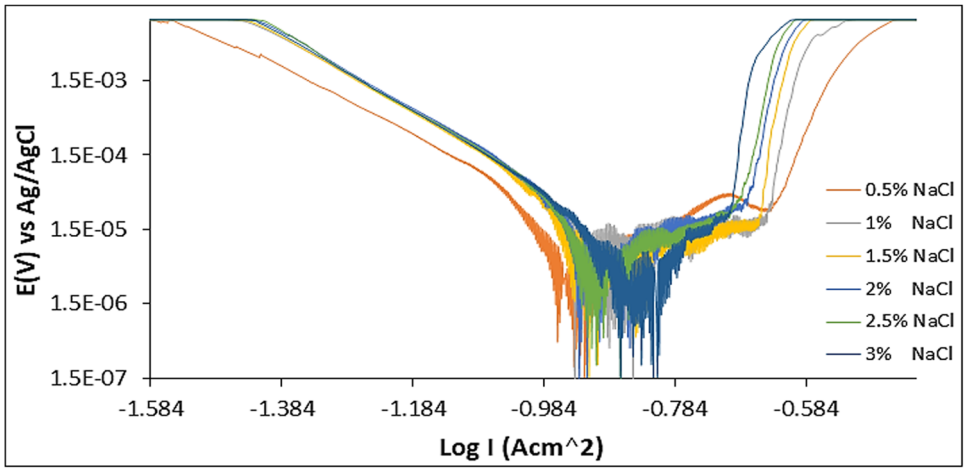

(a)

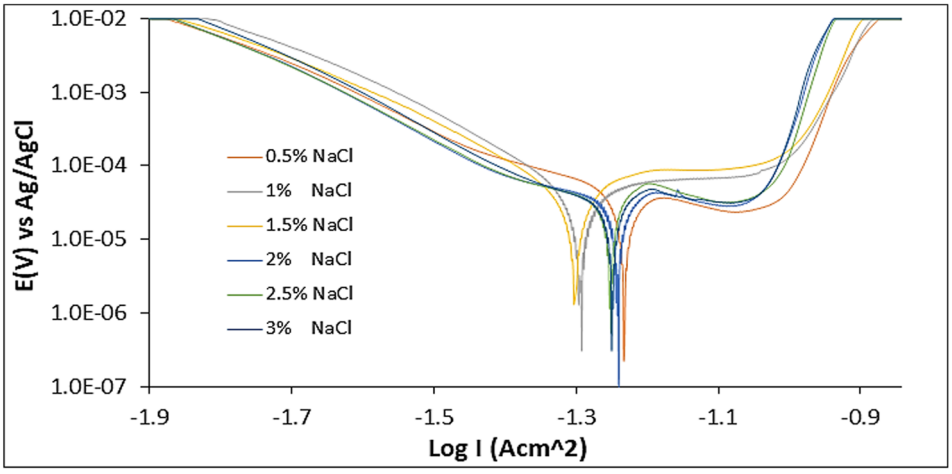

(b)

Figure 1: Potentiodynamic polarization diagram of (a) Al alloy and (b) Zn alloy in neutral chloride media (0.5–3% NaCl concentration).

acid-chloride solutions. The cathodic part of the polarization curves in Figure 1(a) and (b) substantially varies from each other. The plots in Figure 1(a) depict a similar slope configuration after 0.5% NaCl concentration which indicates the cathodic-reduction reaction of the redox reaction process (H_2 evolution and O_2 reduction) occurs under the activation mechanism. The cathodic slope configuration for Zn shows a limited Cl^- anion concentration effect on the cathodic reaction process which invariably alters the corrosion potential of the alloy [55]. Generally, the cathodic reaction occurs according to equations (3)–(5) as follows:

$$2H^+ + 2e^- \rightarrow H_2, \quad (3)$$

$$O_2 + 2H_2O + 4e^- \rightarrow 4OH^-, \quad (4)$$

$$O_2 + 4H^+ + 4e^- \rightarrow 2H_2O. \quad (5)$$

The anodic reaction involves the diffusion of Zn^{2+} and Al^{3+} ions following ionization of the alloy surfaces within the electrolyte [56]. The anodic polarization plots in Figure 1(a) and (b) substantially vary from each other. However, the anodic plots within each figure also vary according to the NaCl concentration. This variation shows the anodic corrosion reaction mechanism is diffusion-controlled. While the plot in Figure 1(b) depicts limited dissolution of the Zn surface due to limited collapse of the inert oxide film initially formed on the alloy before passivation of the alloy [57,58], Al alloy exhibited significant current transient peaks. These peaks signify active-passive transition behavior on the steel surface. The peaks extend to the region where stable pitting initiates for the plots at 1–3% NaCl concentration. A gain in Cl^- ion concentration causes the substitution of OH^- ions on the Al surface resulting probably in the interaction of Cl^- and net progression in corrosion rate as shown in Table 2 [59]. However, the formation of passivating oxide film (Al_2O_3) during potential scanning strongly influenced the overall reaction processes [60–62].

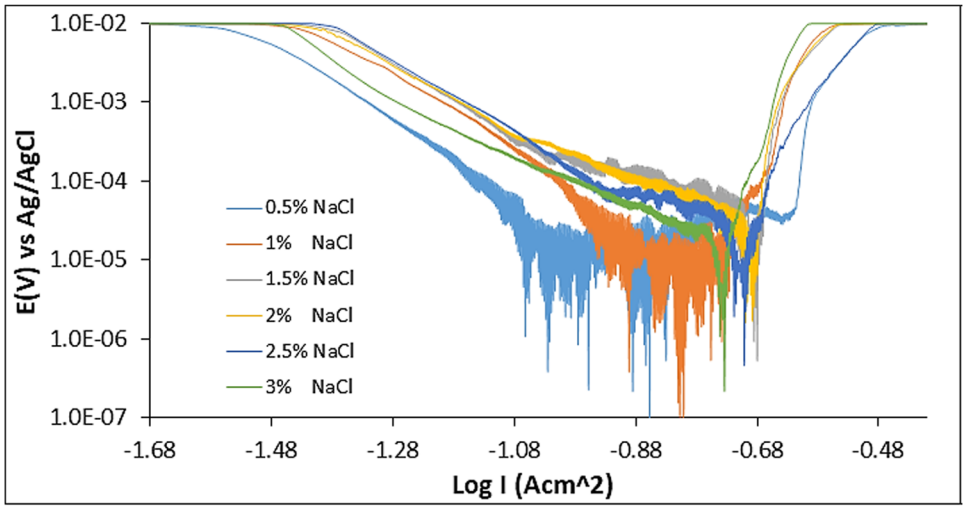

(a)

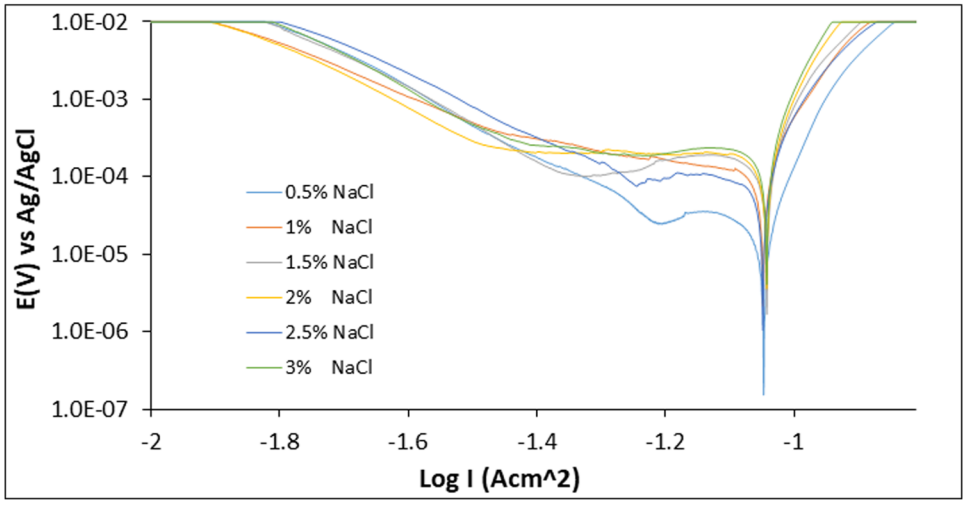

(b)

Figure 2: Potentiodynamic polarization diagram of (a) Al alloy and (b) Zn alloy in 0.0015 M H_2SO_4 media at 0.5–3% NaCl concentration.

The reaction process in the presence of chloride on the Al surface is summarized by the following equation (equations (6)–(13)):

$$Al \rightarrow AI^{3+} + 3e^{-}, \tag{6}$$

$$AI^{3+} + H_2O \rightarrow Al(OH)^{2+} + H^{+}, \tag{7}$$

$$AI^{3+} + Cl \rightarrow AICl^{2+}, \tag{8}$$

$$AI(OH)^{2+} + Cl^{-} \rightarrow AI(OH)Cl^{+}, \tag{9}$$

$$AICl^{2+} + 2H_2O \rightarrow AI(OH)_2CI + 2H^{+}, \tag{10}$$

$$AI(OH)Cl^{+} + H_2O \rightarrow Al(OH)_2CI + H^{+}, \tag{11}$$

$$Al(OH)_2CI + H_2O\ Al(OH)_3 + H^{+} + Cl^{-}, \tag{12}$$

$$2Al(OH)_3(\text{amorphous}) \rightarrow \gamma\ Al_2O_3 \cdot H_2O(\text{boehmite}) + 2H_2O. \tag{13}$$

Zn alloy displays a stable anodic passivation reaction at all Cl^{-} anion concentrations during potential scanning. The analogous anodic reaction process for Zn occurs as follows:

$$Zn \rightarrow Zn^{2+} + 2e^{-}. \tag{14}$$

The strong attraction of Zn alloy for O_2 causes strong resistance to active-passive transition behavior at all NaCl concentrations. The passive portion on Zn stretches to the transpassive portion of the anodic plot where pitting corrosion initiates and grows.

Table 2: Potentiodynamic polarization values for Al and Zn corrosion in neutral chloride media (0.5–3% NaCl concentration)

NaCl conc. (%)	Corrosion rate (mm/year)	Corrosion current (A)	Corrosion current density (A/cm^2)	Corrosion potential (V)	Polarization resistance, R_p (Ω)	Cathodic Tafel slope, B_c (V/dec)	Anodic Tafel slope, B_a (V/dec)
Al alloy							
0	0.031	2.79×10^{-6}	2.79×10^{-6}	−1.019	9201.00	−7.843	4.240
0.5	0.043	3.95×10^{-6}	3.95×10^{-6}	−0.925	6504.00	−13.710	3.019
1	0.062	5.65×10^{-6}	5.65×10^{-6}	−0.848	4725.00	1.446	−1.413
1.5	0.085	7.74×10^{-6}	7.74×10^{-6}	−0.915	3318.00	−7.894	2.963
2	0.084	7.59×10^{-6}	7.59×10^{-6}	−0.930	3408.00	−7.164	13.720
2.5	0.086	7.84×10^{-6}	7.84×10^{-6}	−0.867	3015.00	−19.830	1.601
3	0.082	7.48×10^{-6}	7.48×10^{-6}	−0.814	3814.00	−10.550	4.137
Zn alloy							
0	0.432	2.90×10^{-5}	2.90×10^{-5}	−1.230	886.30	−2.567	−2.737
0.5	0.453	3.04×10^{-5}	3.04×10^{-5}	−1.233	823.20	−2.926	−2.119
1	0.465	3.12×10^{-5}	3.12×10^{-5}	−1.292	796.10	−6.559	2.278
1.5	0.481	3.23×10^{-5}	3.23×10^{-5}	−1.301	723.70	−6.422	2.943
2	0.554	3.72×10^{-5}	3.72×10^{-5}	−1.240	691.40	−2.212	0.046
2.5	0.653	4.38×10^{-5}	4.38×10^{-5}	−1.251	653.20	−2.420	−3.202
3	0.691	4.63×10^{-5}	4.63×10^{-5}	−1.250	586.70	−3.037	−2.941

Table 3: Potentiodynamic polarization values for Al and Zn corrosion in 0.0015 M H_2SO_4 media at 0.5–3% NaCl concentration

NaCl conc. (%)	Corrosion rate (mm/year)	Corrosion current (A)	Corrosion current density (A/cm^2)	Corrosion potential (V)	Polarization resistance, R_p (Ω)	Cathodic Tafel slope, B_c (V/dec)	Anodic Tafel slope, B_a (V/dec)
Al alloy							
0.5	0.037	3.34×10^{-6}	3.34×10^{-6}	−0.857	5811.00	8.056	14.910
1	0.049	4.42×10^{-6}	4.42×10^{-6}	−0.801	7694.00	−1.535	21.120
1.5	0.386	3.51×10^{-5}	3.51×10^{-5}	−0.698	733.10	−0.614	14.400
2	0.384	3.49×10^{-5}	3.49×10^{-5}	−0.698	748.40	−3.414	12.080
2.5	0.385	3.50×10^{-5}	3.50×10^{-5}	−0.701	736.20	−1.236	14.470
3	0.389	3.54×10^{-5}	3.54×10^{-5}	−0.734	721.00	−3.554	32.580
Zn alloy							
0.5	0.465	3.12×10^{-5}	3.12×10^{-5}	−1.047	822.90	−1.756	18.230
1	2.443	1.64×10^{-4}	1.64×10^{-4}	−1.048	156.70	−1.296	12.410
1.5	3.321	2.23×10^{-4}	2.23×10^{-4}	−1.042	115.30	−1.118	11.590
2	3.863	2.59×10^{-4}	2.59×10^{-4}	−1.042	99.12	−1.107	13.700
2.5	4.308	2.89×10^{-4}	2.89×10^{-4}	−1.048	89.62	−2.402	12.010
3	5.016	3.37×10^{-4}	3.37×10^{-4}	−1.042	76.35	−0.554	14.430

Observation of Table 2 shows corrosion rate data for Al and Zn alloys in the neutral chloride solution. Correlation of the data shows Al is more resilient to general corrosion compared to Zn despite significant thermodynamic instability on the Al surface due to current transients. The corrosion rate of Zn started at 0.432 mm/year (0.5% NaCl concentration) analogous to corrosion current density of 2.9×10^{-5} A/cm^2 and consistently increased to 0.691 mm/year (3% NaCl concentration) due to the reaction effect of the Cl^- anions analogous to corrosion current density of 4.63×10^{-5} A/cm^2. The increase in Cl^- anion concentration hastened the resolve of the inert film on Zn alloy such that adsorbed O_2 molecules on the metal surface are substituted by Cl^- anions through aggressive adsorption and removal reactions processes [63]. This exposes the alloy to further corrosion reactions due to the evolution of weak surface precipitates. The corrosion rate of Al alloy initiated at 0.031 mm/year (0.5% NaCl concentration) and consistently increased to 0.085 mm/year at 1.5% NaCl concentration, where it peaked. Beyond 1.5% NaCl concentration, corrosion rate results varied, culminating at 0.082 mm/year consistent with a corrosion current density of 7.48×10^{-6} A/cm^2 at 3% NaCl concentration. The limited variation in corrosion rate

data for Al shows the threshold Cl^- anion concentration was attained from 1.5 to 3% NaCl concentration. The threshold values are the product of the redox reactions on the Al surface and the formation of precipitates.

The corrosion polarization plots in Figure 2(a) and (b) substantially vary from the plots in Figure 1(a) and (b) due to the additional presence of SO_4^{2-} anions within the electrolyte. The dual electrochemical interaction of Cl^- and SO_4^{2-} anions ensured the anodic slope of the polarization curves (Figure 2(a) and (b)) remains high at all Cl^- anion concentrations. This is due to the collapse of the ionized Al and Zn surfaces. This assertion is proven by the corrosion rate results for Al and Zn in Table 3. The corrosion rate results initiated at values of 0.047 and 0.465 mm/year (0.5% NaCl concentration) and consistently progressed to values of 0.389 and 5.016 mm/year. It is clearly stated that the corrosion rate data for Al and Zn in the chloride-sulfate solution are substantially greater than in the neutral chloride solution, while the corrosion rate results for Zn are substantially greater than the corresponding values for Al. The observation proves the chloride-sulfate solution is much stronger and more aggressive than the neutral chloride solution. Second, the precipitates deposited from the reaction processes of the Cl^-/SO_4^{2-} anions are more soluble when compared to the precipitates from the neutral chloride media. The substantial rise in corrosion rate for Al in the chloride-sulfate solution occurred at 1.5% NaCl concentration (0.386 mm/year). The reaction of Al with the SO_4^{2-} anion occurs according to the following equations:

$$Al^{3+} + SO_4^{2-} \rightarrow AlSO_4^{2-}, \quad (15)$$

$$Al(OH)^{2+} + SO_4^{2-} \rightarrow Al(OH)SO_4^{2-}. \quad (16)$$

Zn^{2+} reacts with H^+ ions and SO_4^{2-} ions with respect to the following equations:

$$Zn + H_2SO_4 \rightarrow ZnSO_4 + H_2. \quad (17)$$

Zn^{2+} and $2OH^-$ ions react to produce $Zn(OH)_2$ [64].

$$Zn^{2+} + 2OH^- \rightarrow Zn(OH)_2. \quad (18)$$

Cl^- anions transport to anodic sites resulting in the formation of $Zn_5(OH)_8Cl_2$

$$5Zn(OH)_2 + 2Cl^- + H_2O \rightarrow Zn_5(OH)_8Cl_2{\cdot}H_2O + 2OH^-. \quad (19)$$

The cathodic polarization curves in Figure 2(a) and (b) depict a substantial reduction in the cathodic polarization reaction toward the end of the polarization slope before the intersection with the anodic plot. This is due to a decrease in the H_2 evolution and O_2 reduction reactions associated with enhanced impedance of the alloy surface and a decrease in the diffusion of reducible species [65]. Significant current transients were visible on the anodic cathodic polarization plot due to passivation reactions associated with the transient collapse and passivation of the protective oxide.

3.2 Passivation and pitting corrosion studies

Potentiostatic data for Al and Zn corrosion in a neutral chloride solution were obtained from the potentiodynamic polarization plots. Table 4 depicts the potentiostatic parameters obtained. Al and Zn are known to form protective oxides on their surface when attacked by corrosive species. This occurs due to the interaction of O_2 atoms inside the

Table 4: Potentiostatic data for passivation and pitting corrosion resilience of Al and Zn corrosion in NaCl media (0.5–3% NaCl concentration)

NaCl concentration (%)	Corrosion potential (V)	Passivation potential (V)	Passivation current (A)	Stable pitting potential (V)	Passivation range (V)
Al alloy					
0.5	−0.925	—	—	−0.638	0.287
1	−0.923	—	—	−0.644	0.279
1.5	−0.928	—	—	−0.656	0.272
2	−0.920	—	—	−0.674	0.246
2.5	−0.867	—	—	−0.683	0.184
3	−0.814	—	—	−0.699	0.115
Zn alloy					
0.5	−1.233	−1.200	3.10×10^{-5}	−1.010	0.223
1	−1.250	−1.220	2.68×10^{-5}	−1.050	0.200
1.5	−1.244	−1.210	3.06×10^{-5}	−1.040	0.204
2	−1.240	−1.220	2.70×10^{-5}	−1.040	0.200
2.5	−1.251	−1.230	3.84×10^{-5}	−1.050	0.201
3	−1.250	−1.230	3.08×10^{-5}	−1.050	0.200

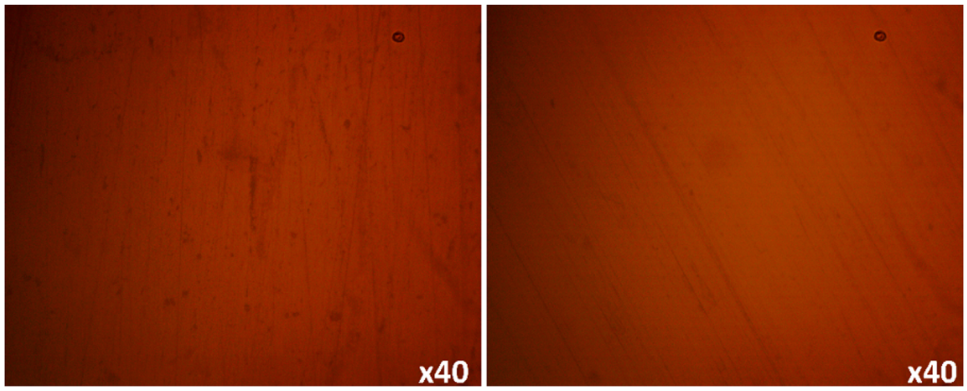

Figure 3: Optical representative images of (a) Al alloy and (b) Zn alloy before corrosion test.

electrolyte. The inert film suppresses electrochemical reactions at the metal-solution interface [66,67]. The corrosion potential is the value where the proportion of cathodic and anodic mechanisms intersects on the polarization plot and indicates their electrochemical properties. The passivation potential represents the potential where transient corrosion pits disappear due to the passivation of the alloy surface [68]. The stable pitting potential is the value at which corrosion pits initiate and grow without the possibility of collapsing while the passivation range gives an indication of the resilience of the protective oxide. Table 4 shows the Al alloy passivates after anodic polarization without the

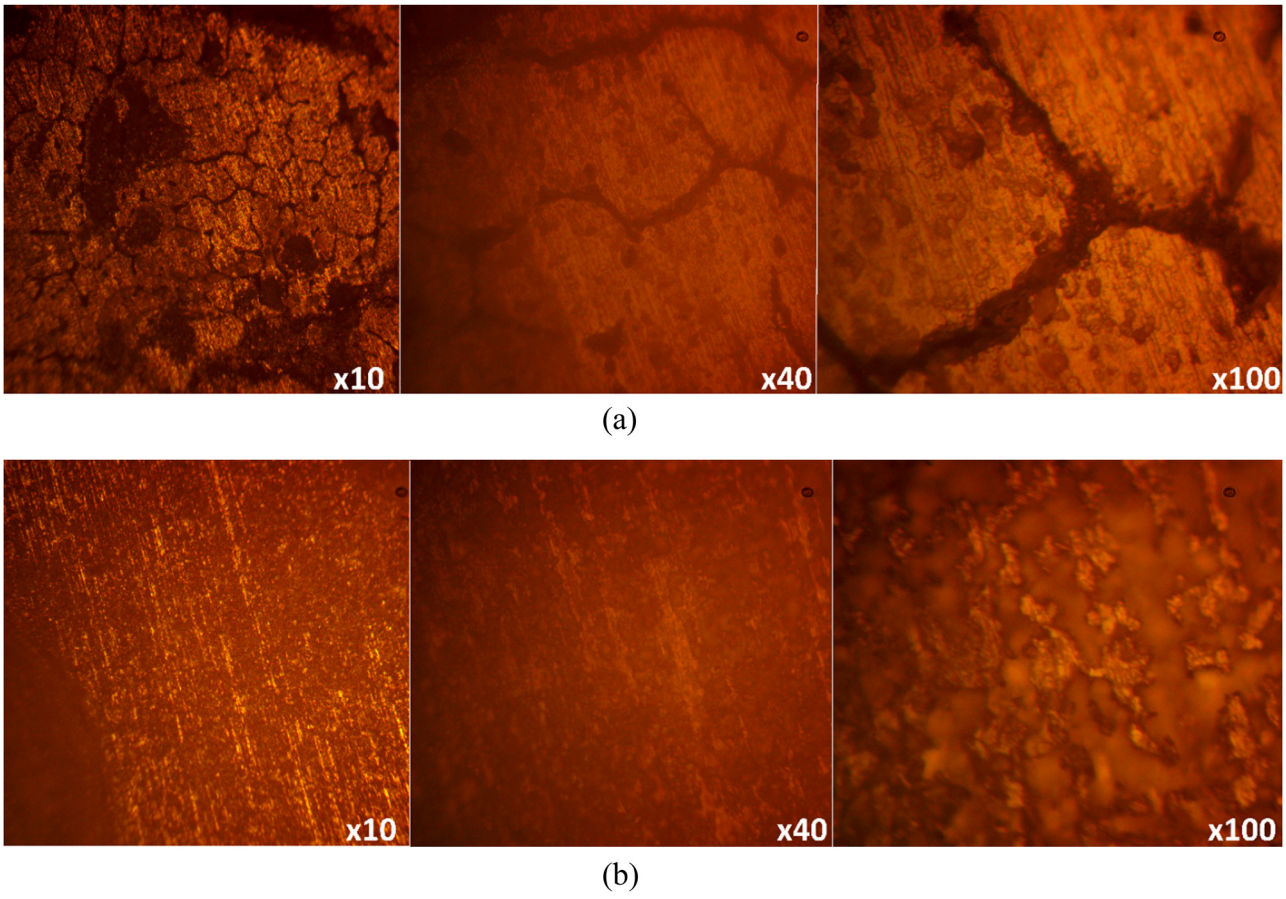

Figure 4: Optical representative images of (a) Al alloy and (b) Zn alloy from neutral chloride solution at 3% NaCl concentration.

evolution of transient corrosion pits (metastable pitting). Hence, its passivation is almost instantaneous. However, significant current transients are visible throughout the passivation region. The current transients are the results of breakage and reformation of the protective oxide on the Al surface. Nevertheless, the protective oxide is thermodynamically unstable.

Comparing these to the potentiostatic data for Zn alloy, it is evident that limited anodic polarization of the alloy surface occurred before stable passivation of the Zn surface. Metastable pitting activity is completely absent from the polarization plots. The absence of current transients shows the protective oxide is stable though it did not translate to greater corrosion resistance considering the corrosion rate values in Table 2. Zn passivated at potential values ranging from −1.20 V (3.10×10^{-5} A) at 0.5% NaCl to −1.23 V (3.08×10^{-5} A) at 3% NaCl concentration. The alloy passivated at almost the same potential which extended up to the potential for stable pitting (−1.010 to −1.050 V). Al pitted at values ranging from −0.638 V at 0.5% NaCl to −0.699 V at 3% NaCl. The passivation range values for Zn alloy are generally lower than the corresponding values for Al alloy as shown in Table 4 at all NaCl concentrations. This confirms that Al though more thermodynamically unstable at the passivated regions exhibits a protective oxide that is more resilient compared to the oxide on Zn [69]. Cl^- anion concentration influences the passivation range for Al alloy. The passivation range value for Al decreases from 0.287 V at 0.5% NaCl to 0.115 V at 3% NaCl. This contrasts the observation for Zn alloy where the passivation range values after 0.5% NaCl concentration (0.223 V) were generally stable till 3% NaCl concentration.

3.3 Optical microscopy analysis

Optical representative images of Al and Zn alloys after corrosion in neutral chloride solution at 3% NaCl concentration are revealed in Figure 3(a) and (b) while Figure 4 shows their representative images from the acid chloride solution at 3% NaCl concentration at mag. ×10, ×40 and ×100. In agreement with the corrosion rate results from potentiodynamic polarization, it is clearly visible in Figure 3(a) that

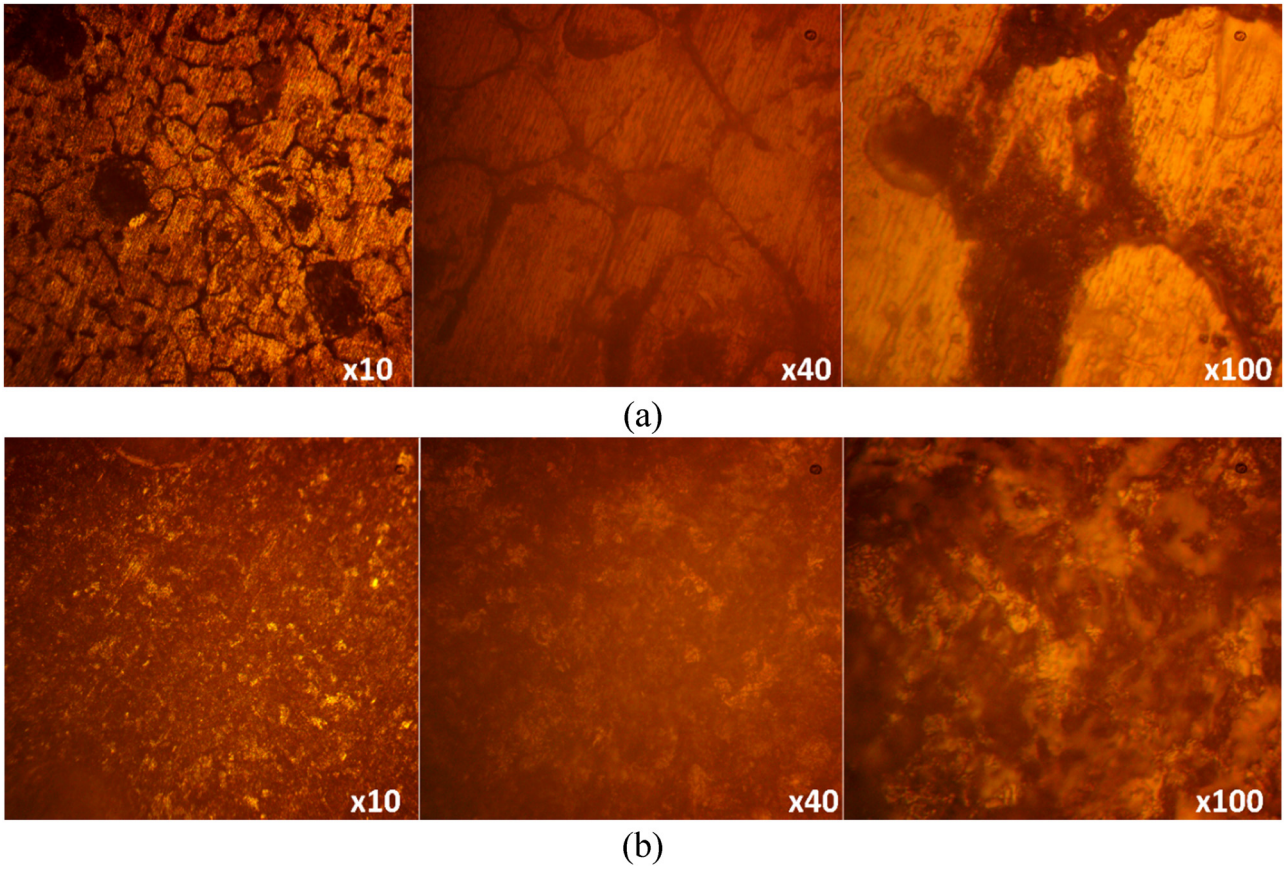

Figure 5: Optical representative images of (a) Al alloy and (b) Zn alloy from acid-chloride solution at 3% NaCl concentration.

localized deterioration occurred on the surface of Al alloy. Localized deterioration occurred along the grain boundary simultaneously with the general surface corrosion. The localized deterioration is responsible for the current transients due to active–passive transition properties of the protective oxide [70]. This phenomenon proves the resilience of the oxide film. However, under-induced potential corrosion will eventually occur. Comparing this to the optical image in Figure 3(b), it is established that Zn underwent general surface deterioration. The effect of localized corrosion is negligible. This is due to the microstructural and metallurgical properties of Zn which significantly differs from Al alloy. The extent of localized surface deterioration on Al increased in the presence of combined Cl^- and SO_4^{2-} anions as shown in Figure 4(a). Adsorbed O_2 atoms responsible for the formation of Al_2O_3 were displaced by the corrosive anions which exposed the substrate Al alloy to corrosion. This observation also applies to Zn as depicted in Figure 4(b) where the degree of general surface deterioration is much higher.

3.4 Open circuit potential analysis

Open circuit potential plots for Al and Zn at 0.5% and 3% NaCl concentrations from the neutral chloride and acid-chloride solutions were produced as shown in Figures 5(a) and (b). In agreement with the results from potentiodynamic polarization test, Figure 5(a) shows Al alloy in neutral chloride solution displayed greater corrosion resilience and increased protective oxide evolution during potential monitoring. The plot at 0.5% NaCl concentration

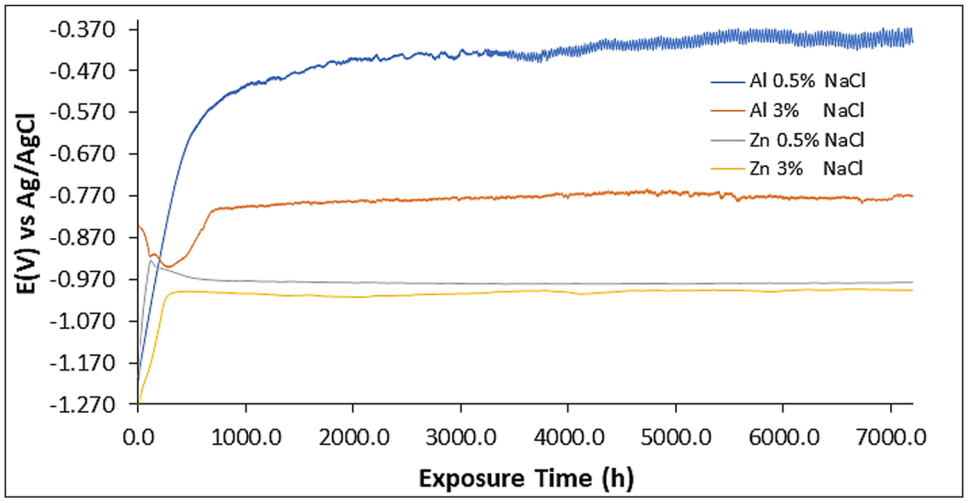

(a)

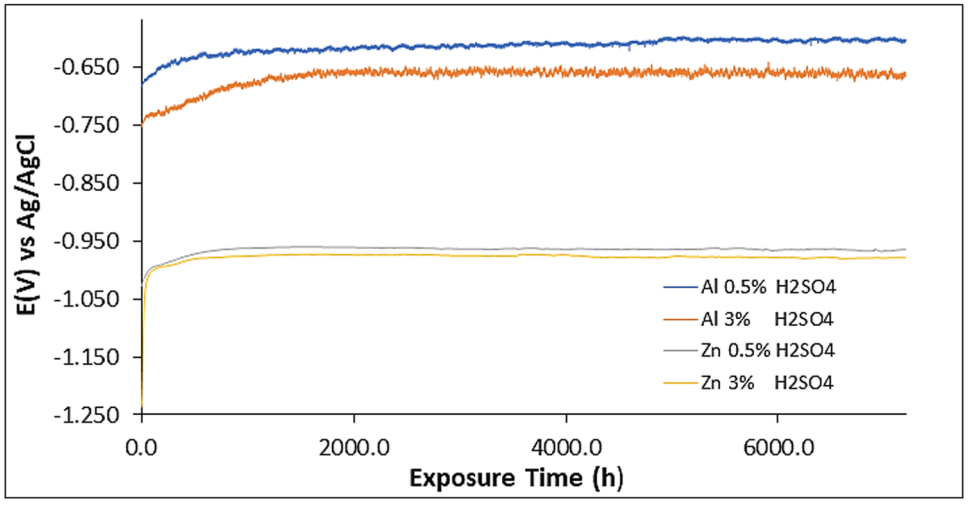

(b)

Figure 6: OCP Plot for Al and Zn alloys in (a) neutral chloride solution and (b) acid-chloride solution at 0.5 and 3% NaCl concentration.

initiated at −1.216 V (0 s), a significant electronegative value due to its amphoteric nature. The surface characteristics of the Al results in spontaneous electrochemical reactions, i.e. instantaneous collapse and subsequent repassivation of the protective oxide. Electropositive shift of the OCP plot occurred to 901.8 s (−0.524 V). It must be noted that the shift is due to the growth of Al_2O_3 on Al alloy [71]. The competitive reaction of O_2 and Cl^- ionic species results on the alloy surface results in adsorption of O_2 atoms responsible for oxide formation. Though this observation is specific to 0.5% NaCl concentration. Beyond 900 s of exposure, the OCP plot for Al is relatively stable, but the potential transients show the electrochemical properties of the protective oxide is unstable till 7,200 s at −0.399 V. Comparing these observations to the plot at 3% NaCl concentration, it is very probable that increase in Cl^- anion concentration increased the corrosion tendency of the Al alloy as depicted in the plot configuration [Figure 6(a)]. The electropositive shift associated with Al at 5% NaCl concentration has significantly decreased. The plot at 3% NaCl concentration initiated at −0.844 (0 s), underwent a minor electronegative shift till −0.948 V at 269.6 s before shifting electropositively to −0.801 V at 808.21 s. Henceforth, from this value, the OCP plot was thermodynamically stable till −0.771 V at 7,200 s. It is also visible that the potential transients have decreased.

Comparing the thermodynamic behavior of Al to Zn in NaCl, Zn at 0.5, and 3% NaCl concentration displayed the same OCP plot configuration. The plots initiated at −1.205 and −1.268 V shifted electropositively before reaching thermodynamic equilibrium at −0.929 V (132.4 s) and −1.007 V (282.8 s). The corrosion rate values at 7,200 s are −0.977 and −0.996 V which is significantly more electronegative than the corresponding values for Al alloy. However, potential transients are completely absent due to the stability of the protective oxide on Zn in spite of its higher corrosion tendency. The plot configuration for Zn in the acid-chloride solution at 0.5 and 3% NaCl concentration [Figure 6(b)] was usually the same as that of Zn in the neutral chloride solution [Figure 6(a)]. The OCP values started at −1.03 and −1.24 V (0 s) and underwent a sharp electropositive shift to −0.990 V at 200 s. After this section, the OCP plot was generally constant till −0.96 and −0.98 V at 7,200 s. In the presence of the combined electrochemical influence of Cl^- and SO_4^{2-} anions, the electrochemical properties of the Zn surface were generally stable. The OCP plot for Al in the acid-chloride solution exhibited substantial potential transient throughout. The degree of instability is much higher for the Al plot at 3% NaCl concentration. Both plots (Al at 0.5 and 3% NaCl concentration) initiated at −0.684 and −0.753 V (0 s) and terminated at −0.602 and −0.666 V (7,200 s)

4 Conclusion

Analysis of the corrosion resistance and passivation behavior of aluminum and zinc alloys in neutral chloride and acid chloride solutions shows the protective oxide on aluminum is more resilient to general and localized deterioration in the presence of Cl^- and SO_4^{2-} anions. The corrosion potential of zinc polarization plots was significantly more electronegative compared to the values for aluminum. The passivation range values for aluminum were significantly wider than the values for zinc despite visible thermodynamic instability. Data from open circuit potential measurement show significant formation and growth of the protective oxide aluminum which is responsible for its higher corrosion resistance compared to zinc. Zinc alloy despite its lower corrosion resistance compared to aluminum exhibited thinner and less resilient oxide formation which exhibits more thermodynamic stability. Localized deterioration occurred along the grain boundary simultaneously with the general surface corrosion on the surface of Al alloy. The deterioration is responsible for the significant current transients on the polarization plots. Zn underwent general surface deterioration which became more adverse in the presence of Cl^-/SO_4^{2-} anions. This phenomenon is due to differences in the microstructural and metallurgical properties of Zn compared to Al alloy.

Acknowledgement: The author is grateful to Covenant University for their financial support and provision of facilities towards the success of this research.

Conflict of interest: Author states no conflict of interest.

Data availability statement: The datasets generated during and/or analysed during the current study are available from the corresponding author on reasonable request.

References

[1] Serosh E, Bernd H, Volker S. A review of the development and application of microalloyed medium carbon steels. Steel Res. 1987;58(8):369–76.

[2] Han D, Xinjun S. Deformation induced ferrite transformation in low carbon steels. Curr Opin Solid State Mater Sci. 2008;9(6):269–76.

[3] Deepak D, Kateřina L, Thomas B. Carbon steel corrosion: A review of key surface properties and characterization methods. RSC Adv. 2017;7:4580–610.

[4] Siddiqui RA, Hussein AA. Hydrogen embrittlement in 0.31% carbon steel used for petrochemical applications. J Mater Process Technol. 2005;170(1–2):430–5.

[5] Edmonds DV, Cochrane RC. The effect of alloying on the resistance of carbon steel for oilfield applications to CO_2 corrosion. Mater Res. 2005;8(4). doi: 10.1590/S1516-14392005000400004.
[6] Loto RT. Anti-corrosion performance of the synergistic properties of benzenecarbonitrile and 5-bromovanillin on 1018 carbon steel in HCl environment. Sci Rep. 2017;7(1):17555. doi: 10.1038/s41598-017-17867-0.
[7] Faisal M, Gusai A, Erin VI, Keller MW, Shirazi S, Roberts KP. Mechanistic modeling of erosion–corrosion for carbon steel. In Trends in oil and gas corrosion research and technologies. Sawston, Cambridge: Woodhead Publishing; 2017. p. 749–63. doi: 10.1016/B978-0-08-101105-8.00031-0.
[8] Cai J, Sun L, Ma H, Xiaogang L. Corrosion characteristics of Q690qE high-strength bridge steel in simulated coastal–industrial environment and its influence on mechanical and corrosion fatigue behaviors. Constr Build Mater. 2002;341:127830. doi: 10.1016/j.conbuildmat.2022.127830.
[9] Zhang W, Yang S, Wen-Tong G, Qiang H, Lujun Z. Corrosion behavior of the low alloy weathering steels coupled with stainless steel in simulated open atmosphere. Mater Chem Phys. 2022;288:126409. doi: 10.1016/j.matchemphys.2022.126409.
[10] Loto RT. Electrochemical analysis of the corrosion inhibition properties of 4-hydroxy-3-methoxybenzaldehyde on low carbon steel in dilute acid media. Cogent Eng. 2016;3(1):1242107.
[11] Loto RT. Pitting corrosion evaluation and inhibition of stainless steels: A review. J Mater Environ Sci. 2015;6(10):2750–62.
[12] Ping L, Min D. Effect of chloride ion content on pitting corrosion of dispersion-strengthened-high-strength steel. Corros Commun. 2022;7:23–34. doi: 10.1016/j.corcom.2022.03.005.
[13] Kuklík V, Kudláček J. List of selected zinc coating technologies. In Hot-dip galvanizing of steel structures. Amsterdam: Elsevier; 2016. p. 1–5. doi: 10.1016/C2014-0-03512-5.
[14] Zhang XG. Corrosion of zinc and zinc alloys. In ASM HandBook. Corrosion: Materials. Boca Raton, Florida: CRC Press; Vol 13B. 2005. doi: 10.31399/asm.hb.v13b.a0003830.
[15] Zinc Statistics and Information. National Minerals Information Center. https://www.usgs.gov/centers/national-minerals-information-center/zinc-statistics-and-information. Retrieved November 3, 2022.
[16] Greenwood NN, Earnshaw A. Chemistry of the elements. 2nd edn. Oxford: Butterworth-Heinemann; 1997.
[17] Emsley J. “Zinc”. Nature’s building blocks: An A-Z guide to the elements. Oxford, England: Oxford University Press; 2001. p. 499–500.
[18] Zhang XG. Corrosion and electrochemistry of zinc. New York: Springer; 1996. p. 93.
[19] Cook AR. Zinc and the protection of offshore structures. Offshore Technology Conference. Houston, Texas; 1969. doi: 10.4043/1040-MS.
[20] Veleva L, Meraz E, Acosta M. Zinc precipitation runoff from galvanized steel in humid tropical climate. Corros Eng Sci Technol. 2010;45(1):76–83. http://www.doi.org/10.1179/174327809X457030.
[21] Loto RT, Babalola PO. Corrosion polarization behavior and microstructural analysis of AA1070 aluminium silicon carbide matrix composites in acid chloride concentrations. Cogent Eng. 2017;4:1422229. doi: 10.1080/23311916.2017.1422229.
[22] Birbilis NT, Muster TH, Buchheit RG. Corrosion of aluminium alloys in corrosion mechanisms in theory and practice. 3rd edn. Boca Raton, Florida: CRC Press; 2011. p. 705–36.
[23] Zhang Z, Yang X, Zhang J, Zhou G, Xu X, Zou B. Effect of welding parameters on microstructure and mechanical properties of friction stir spot welded 5052 aluminum alloy. Mater Des. 2011;32:4461–70.
[24] The aluminium association. https://aluminum.org/aluminum-advantage/facts-glance.
[25] Alaneme KK, Olubambi PA, Afolabi AS, Bodurin MO. Corrosion and tribological studies of bamboo leaf ash and alumina reinforced Al-Mg-Si alloy matrix hybrid composites in chloride medium. Int J Electrochem Sci. 2014;9:5663–74. http://www.electrochemsci.org/papers/vol9/91005663.pdf.
[26] Asif M, Chandra K, Misra PS. Development of aluminium based hybrid metal matrix composites for heavy duty applications. J Miner Mater Charact Eng. 2011;10:1337–44.
[27] Prasad DS, Shoba C, Ramanaiah N. Investigations on mechanical properties of aluminum hybrid composites. J Mater Res Technol. 2014;3:79–85.
[28] Staley JT. Corrosion of aluminium aerospace alloys. Mater Sci Forum. 2016;877:485–91.
[29] Veleva L, Kane RD. Atmospheric corrosion. In ASTM Handbook. Vol. 13A. Materials Park, Ohio: ASM International; 2003. p. 196–209.
[30] Wallinder O, Leygraf C. A critical review on corrosion and runoff from zinc and zinc-based alloys in atmospheric environments. Corrosion. 2017;73(9):1060–77. doi: 10.5006/2458.
[31] Davis JR. Corrosion of aluminum and aluminum alloys. Materials Park, Ohio: ASM International; 1999. https://www.asminternational.org/documents/10192/1849770/06787G_Sample.pdf/c4151917-99fc-46e8-a310-d5578d0af160.
[32] Smith WJ, Goodwin FE. Hot dip coatings. Reference module in materials science and materials engineering. Amsterdam: Elsevier; 2017. doi: 10.1016/B978-0-12-803581-8.09214-6.
[33] Hurlen T, Lian H, Odegard OS, Valand TV. Corrosion and passive behaviour of aluminium in weakly acid solution. Electrochim Acta. 1984;29:579–85.
[34] Mountarlier V, Gigandet MP, Normand B, Pagetti J. EIS characterisation of anodic films formed on 2024 aluminium alloy, in sulphuric acid containing molybdate or permanganate species. Corros Sci. 2003;47:937–51.
[35] Lukovits I, Kalman E, Zucchi F. Corrosion inhibitors—Correlation between electronic structure and efficiency. Corrosion. 2001;57:3–9.
[36] Brett CMA, Gomes IAR, Martins JPS. The electrochemical behaviour and corrosion of aluminium in chloride media. The effect of inhibitor anions. Corros Sci. 1994;36:915–23.
[37] Solange PD, Benjamín HP, Rosario ÁG, Mauro BV. Study of pitting corrosion of the commercial aluminium alloy AA3003 in saline environment. Rev Tec Fac Ing Univ. 2011;34:108–23. http://ve.scielo.org/scielo.php?pid=S0254-07702007000400020&script=sci_abstract&tlng=en.
[38] Natishana PM, O’Grady WE. Chloride ion interactions with oxide-covered aluminum leading to pitting corrosion: A review. J Electrochem Soc. 2014;161:C421–32.
[39] Szklarska-Smialowska Z. Pitting corrosion of aluminium. Corros Sci. 1999;41:1743–67.
[40] Zaid B, Saidi D, Benzaid A, Hadji S. Effects of pH and chloride concentration on pitting corrosion of AA6061 aluminum alloy. Corros Sci. 2008;50:1841–7.
[41] Bolzoni F, Contreras G, Lazzari L, Ormellese M, Pérez E, Re G, et al. Influence of chloride and sulphate content on the performance of aluminium based galvanic anodes. Corros Rev. 2011;29:287–96.

[42] Leckie HP, Uhlig HH. Environmental factors affecting the critical potential for pitting in 18–8 stainless steel. J Electrochem Soc. 1996;113:1262–7.
[43] Baer DR. Protective and non-protective oxide formation on 304 stainless steel. Appl Surf Sci. 1981;7(1–2):69–82. doi: 10.1016/0378-5963(81)90061-1.
[44] Graedel TE. Corrosion mechanisms for zinc exposed to the atmosphere. J Electrochem Soc. 1989;136(4).
[45] Ferry M, Mohd Sukarnoor NI. Study of corrosion performance of zinc coated steel in seawater environment. Indones J Nav Archit. 2013;1:1.
[46] Yaw-Tzong TH, Jian Hong L, Jyh Wei H, Jyh Hwa W, Ting Chung C, Han Chang S, et al. Corrosion behavior of zinc and aluminum coated steels in marine environments of Taiwan. San Diego, California: NACE CORROSION; 2003.
[47] Al-Moubaraki AH, Al-Rushud HH. The Red sea as a corrosive environment: Corrosion rates and corrosion mechanism of aluminum alloys 7075, 2024, and 6061. Int J Corros. 2018;2018:2381287. doi: 10.1155/2018/2381287.
[48] Seyeuxa A, Zannaa S, Allion A, Marcus P. The fate of the protective oxide film on stainless steel upon early stage growth of a biofilm. Corros Sci. 2015;91:352–6. doi: 10.1016/j.corsci.2014.10.051.
[49] Silva R, Kugelmeier CL, Vacchi GS, Martins Junior CB, Dainezi I, Afonso CRM, et al. A comprehensive study of the pitting corrosion mechanism of lean duplex stainless steel grade 2404 aged at 475 °C. Corros Sci. 2021;191:109738. doi: 10.1016/j.corsci.2021.109738.
[50] Mollapour Y, Poursaeidi E. Experimental and numerical analysis of pitting corrosion in CUSTOM 450 stainless steel. Eng Fail Anal. 2021;128:105589. doi: 10.1016/j.engfailanal.2021.105589.
[51] Pao L, Muto I, Sugawara Y. Pitting at inclusions of the equiatomic CoCrFeMnNi alloy and improving corrosion resistance by potentiodynamic polarization in H_2SO_4. Corros Sci. 2021;191:109748. doi: 10.1016/j.corsci.2021.109748.
[52] Zhang X, Zhao S, Wang Z, Li J, Qiao L. The pitting to uniform corrosion evolution process promoted by large inclusions in mooring chain steels. Mater Charact. 2022;181:111456. doi: 10.1016/j.matchar.2021.111456.
[53] Liu R, Hurley M, Kvryan A, Williams G, Scully JR, Birbilis N. Controlling the corrosion and cathodic activation of magnesium via microalloying additions of Ge. Sci Rep. 2016;6:28747. doi: 10.1038/srep28747.
[54] Calderón JP, Reyes Barragán JL, Barraza Fierro JI, Cruz Mejía H, Arrieta González CD, Ravelero Vázquez V, et al. Corrosion behavior of Al modified with Zn in chloride solution. Materials. 2022;15:4229. doi: 10.3390/ma15124229.
[55] Foly RT. Complex ions and corrosion. J Electrochem Soc. 1975;122(11):1493. doi: 10.1149/1.2134051.
[56] Bhattamishra AK, Banerjee MK. Corrosion behaviour of Al-Zn-Ms alloys in NaCl solution in presence of cerium salts. Int J Mater Res. 1993;84(10):734–6. doi: 10.1515/ijmr-1993-841015.
[57] Koroleva EV, Thompson GE, Hollrigl G, Bloeck M. Surface morphological changes of aluminium alloys in alkaline solution: Effect of second phase material. Corros Sci. 1999;41(8):1475–95. doi: 10.1016/S0010-938X(98)00188-7.
[58] Moon SM, Pyun SI. The corrosion of pure aluminium during cathodic polarization in aqueous solutions. Corros Sci. 1997;39(2):399–408. doi: 10.1016/S0010-938X(97)83354-9.
[59] Vargel C. The influence of oxygen dissolved in water. Corrosion of aluminium. Amsterdam: Elsevier; 2004. doi: 10.1016/B978-0-08-044495-6.X5000-9.
[60] Aziz I, Qi Z, Min X. Corrosion inhibition of SiCp/5A06 aluminum metal matrix composite by cerium conversion treatment. Chin J Aeronaut. 2009;22(6):670–6. doi: 10.1016/S1000-9361(08)60157-0.
[61] Trowsdale AJ, Noble B, Harris SJ, Gibbins ISR, Thompson GE, Wood GC. The influence of silicon carbide reinforcement on the pitting behaviour of aluminium. Corros Sci. 1996;38(2):177–91. doi: 10.1016/0010-938X(96)00098-4.
[62] Mouanga M, Ricq L, Douglade G, Douglade J, Berçot P. Influence of coumarin on zinc electrodeposition. Surf Coat Technol. 2006;201:762–7.
[63] Christopher LA, Chao L, Ali A, Ryan MK, Robert GK, Jacob C, et al. Oxygen reduction on stainless steel in concentrated chloride media. J Electrochem Soc. 2018;165:C869. http://www.doi.org/10.1149/2.0181813jes.
[64] Ralston KD, Fabijanic D, Birbilis N. Effect of grain size on corrosion of high purity aluminium. Electrochim Acta. 2011;56:1729. doi: 10.1016/j.electacta.2010.09.023.
[65] Serna LM, Zavadil KR, Johnson CM, Wall FD, Barbour JC. A critical implanted Cl concentration for pit initiation on aluminum thin films. J Electrochem Soc. 2006;153:B289. doi: 10.1149/1.2205172.
[66] Tang Y, Zuo Y. The metastable pitting of mild steel in bicarbonate solutions. Mater Chem Phys. 2004;88(1):221–6. doi: 10.1016/j.matchemphys.2004.07.01.
[67] Li Q, Jensen JO, Bjerrum NJ. Chemistry, electrochemistry, and electrochemical applications: Aluminum. In Encyclopedia of electrochemical power sources. Amsterdam: Elsevier; 2009. p. 695–708. doi: 10.1016/B978-044452745-5.00951-5.
[68] Hugh SI, Yuichi I. Current and potential transients during localized corrosion of stainless-steel. J Electrochem Soc. 1985;132(6):1288. http//www.doi.org/10.1149/1.2114104.
[69] Zhang L, Duan Y, Gao R, Yang J, Wei K, Tang D, et al. The Effect of potential on surface characteristic and corrosion resistance of anodic oxide film formed on commercial pure titanium at the potentiodynamic-aging mode. Materials (Basel). 2019;12(3):370, http://www.doi.org/10.3390/ma12030370.
[70] Taylor CD, Li S, Samin AJ. Oxidation versus salt-film formation: Competitive adsorption on a series of metals from first-principles. Electrochim Acta. 2018;269:93–101. doi: 10.1016/j.electacta.2018.02.150.
[71] Yin X, Wang H, Sun S, Han E. Comparative study on the adsorption behaviors of O and Cl on Fe(110) surfaces with different Cr content. Mater Today Commun. 2020;24:101122. doi: 10.1016/j.mtcomm.2020.101122.